Modeling and numerical simulation of the nonlinear dynamics of the forced planar string pendulum

by

Veronica Ciocanel

Department of Mathematics
Duke University

Date: _____

Approved:

_____
Thomas Witelski, Supervisor

Dissertation submitted for Graduation with Distinction
in the Department of Mathematics
at Duke University, Durham, NC
2012

Abstract

Modeling and numerical simulation of the nonlinear dynamics of the forced planar string pendulum

by

Veronica Ciocanel

Department of Mathematics
Duke University

Date: _____

Approved:

_____
Thomas Witelski, Supervisor

An abstract of a dissertation submitted for
the Graduation with Distinction in the Department of Mathematics
Mathematics of Duke University
2012

Abstract

The string pendulum consists of a mass attached to the end of an inextensible string which is fastened to a support. Analyzing the dynamics of such forced supports is motivated by understanding the behavior of suspension bridges or of tethered structures during earthquakes. Applying an external forcing to the pendulum's support can cause the pendulum string to go from taut to slack states and vice versa, and is capable of exhibiting interesting periodic or chaotic dynamics. The inextensibility of the string and its capacity to go slack make simulation and analysis of the system complicated. The string pendulum system is thus formulated here as a piecewise-smooth dynamical system using the method of Lagrange multipliers to obtain a system of differential algebraic equations (DAE) for the taut state.

In order to find a formulation for the forced string pendulum system, we first turn to similar but simpler pendulum systems, such as the classic rigid pendulum, the elastic spring pendulum and the elastic spring pendulum with piecewise constant stiffness. We perform a perturbation analysis for both the unforced and forced cases of the spring pendulum approximation, which shows that, for large stiffness, this is a reasonable model of the system. We also show that the spring pendulum with piecewise constant stiffness can be a good approximation of the string pendulum, in the limit of a large extension constant and a low compression constant. We indicate the behavior and stability of this simplified model by using numerical computations of the system's Lyapunov exponents. We then provide a comparison of the spring

pendulum with piecewise constant stiffness with the formulation of the taut-slack pendulum using the DAE for the taut states and derived switching conditions to the slack states.

Contents

List of Figures

Acknowledgements

This paper is a result of the work done for the Duke University PRUV Fellowships program during summer 2010, the Math 192 independent study taken during Spring 2011, and the Math 194 research independent study taken under the guidance of professor Thomas Witelski. I would also like to thank Professor David Schaeffer for the useful suggestions for my thesis. This work was supported by an NSF CMMI grant 0927186: "New challenges in Non-smooth Dynamical systems".

1

Introduction

The string pendulum, which consists of a mass suspended by a string, is a seemingly simple system displaying interesting behavior when under the application of various external forces. Modeling this system can become challenging if we consider that the string can become slack and investigate its stability behavior. The forced string pendulum problem introduces changes of states that determine the non-smooth character of the system, thus leading to ODE's with switching forms, which might only be piecewise smooth [12]. Kinematic constraints or physical effects such as friction, impacts or backlash are known to cause non-smooth phenomena which represent a challenge for engineers and mathematicians [12]. Moreover, since these problems are nonlinear, chaotic motions can appear and one can find when they occur.

Simpler systems such as the classic pendulum have been studied extensively. The planar classic pendulum with vertical periodic forcing was studied in [1], and its sensitivity to initial conditions was inspected by looking at the system's Lyapunov exponents. In [5], it was shown that for large-enough velocities, the string pendulum will become slack and the mass will follow a parabolic path for projectile motion. Taut-slack states can occur in this situation, however no external forcing is consid-

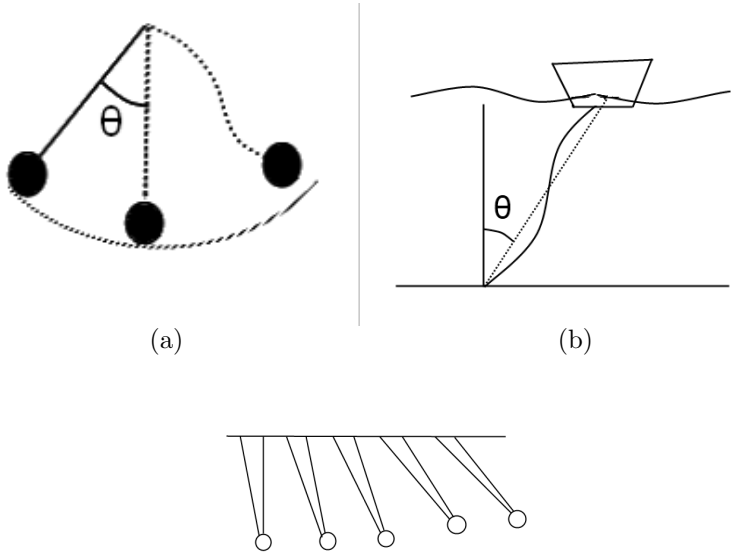

(a) (b)

(c)

FIGURE 1.1: A string pendulum (a) and its applications such as (b) moored boats and (c) Newton's cradle

ered. In [8], the motion of a jogger's ponytail is modeled using first a rigid string and then a flexible string under periodic vertical forcing, but the stability of the system is not discussed. An experimental approach to analyze the behavior of two cables attached to a rigid frame and shaken horizontally was proposed in [16].

1.1 Applications

We consider basic mechanical systems of pendulums, as well as use the physical understanding of the system to guide us to mathematical approximations of the string forced pendulum. This work is motivated by broader applications to ODE's with switching forms and also to specific extensions of the forced string pendulum. One application is Newton's cradle, which is a desktop toy that shows the effects of conservation of energy and momentum, as well as those of friction and air resistance. It usually consists of 5 metal balls which are touching at rest, each suspended by

strings from a common rigid frame, see Fig. 1.1(c). This toy is usually observed for its reaction to the action of pulling one or two of its exterior balls and letting them collide. However, more interesting dynamics involving impacts and chaotic motion can be noticed when pulling one or two balls sideways so that one of the strings is taut and one slack [16]. Moreover, the behavior of the system when the whole frame is moved either horizontally or vertically with a given forcing can be of interest. Similarly, analyzing the dynamics of structures during earthquakes could benefit from a study of forced frames.

Another application could include moored boats, which are fastened to a fixed object by a rope, see Fig. 1.1(b). Boats anchored during storms could undergo backlash and become loose if the rope is fully extended, thus becoming analogous to the model of a pendulum with loose string. Another example of a system with switching behavior is that of suspension bridges, whose loads are hung on suspension cables. These cables are normally linear at equilibrium, but if shaking occurs they can slacken, leading to piecewise defined characteristics [6].

1.2 Overview

Our main goal is to explain and analyze the interesting dynamics of the string pendulum with forced frame. We first considered the classic pendulum and calculated the equations of motion using the approximation given by a spring pendulum with large spring constant in Chapter 3. This formulation using the spring pendulum was previously considered in [5], but only for the unforced case. This spring pendulum approximation is verified by the perturbation analysis for small amplitude oscillations (Chapter 3.3) and for the limit of large spring constant (Chapter 3.4). We then adjusted this model to a spring pendulum with piecewise constant stiffness formulation in Chapter 3.5. A similar approach using an elastic pendulum with piecewise constant stiffness was considered in [8], but the question of stability was only an-

swered there for lateral perturbations of the motion. To our knowledge, no previous work was done to model the string pendulum using a system of DAE's for the taut state and switching conditions to the slack state (Chapter 4 and 5). Numerical simulations of these formulations provide phase planes and time profiles of the x and z components. [1] uses Lyapunov exponents to look at the stability of the planar classic pendulum with vertical forcing. Using numerical simulations, we determine Lyapunov exponents for all the formulations of the system to show chaotic and periodic behavior for different ranges of forcing, which is not accomplished in previous papers. With the agreement of time profiles and of the Lyapunov exponents, we show that the classic, spring pendulum and DAE formulations of the rigid pendulum match very closely. Moreover, the spring pendulum with piecewise constant stiffness and the taut-slack formulation have similar dynamics for the same forcing amplitudes (Chapter 6).

We start by analyzing the dynamics of the classic pendulum with forcing in Chapter 2. Chapter 3 is dedicated to the modeling of the classic and taut/slack pendulum using an elastic spring pendulum. Chapter 4 shows the modeling of the classic pendulum system using a DAE system to impose the geometric constraint of fixed length. The changes that need to be considered when switching to the taut/slack pendulum system are analyzed in Chapter 5. Lastly, Chapter 6 provides a comparison of the DAE and spring pendulum models of the taut/slack case. In appendix A, we calculate the switching conditions for the three-dimensional case of a string pendulum, which will be useful in future work.

2

Preliminaries and background results

2.1 Review of the Euler-Lagrange formulation

We begin by describing the method used to derive the equations of motion of simple problems involving a pendulum.

Hamilton's principle is an approach for formulating the governing equations for a system. These equations are equivalent to those derived from Newtonian mechanics and can thus be used in cases where Newton's equations are difficult to obtain directly [9].

We begin by defining $\mathcal{L}$ as the Lagrangian, which equals

$$\mathcal{L} = T - U, \tag{2.1}$$

where T is the kinetic energy and U is the potential energy of the system. This becomes meaningful in the mechanical problems where Hamilton's principle of Least Action is applied. The principle states that the dynamics of a physical system are determined by a variational problem for a functional based on a single function: the Lagrangian defined above. The principle of least action gives equations of motion of a mechanical system for the dynamical solution that minimizes the action integral,

defined as $\int_0^T \mathcal{L}dt$.

The mathematics involved in carrying out the principle is given by the theory of calculus of variations, which deals with finding extremes of functionals. The goal is thus to find those functions that are local minimizers/critical points of the functional [11].

Now consider the functional I defined as

$$I = \int_a^b \mathcal{L}(t, y_* + \epsilon h, \frac{dy_*}{dt} + \epsilon \frac{dh}{dt})dt, \tag{2.2}$$

with y_* being the optimal solution, we can expand the function under the integral as a Taylor series for $\epsilon \to 0$ (h is a variation as a function of t).

The functional becomes

$$I \sim \int_a^b \mathcal{L}_* dt + \epsilon \int_a^b \left(\frac{\partial \mathcal{L}}{\partial y} h + \frac{\partial \mathcal{L}}{\partial \dot{y}} \dot{h} \right) dt + O(\epsilon^2).$$

To find a critical point of the above, we need to set the second integral equal to 0 for all variations $h(t)$:

$$\int_a^b \left(\frac{\partial \mathcal{L}}{\partial y} h + \frac{\partial \mathcal{L}}{\partial \dot{y}} \dot{h} \right) dt = 0.$$

Integration by parts leads to

$$\frac{\partial \mathcal{L}}{\partial \dot{y}} h \Big|_a^b + \int_a^b \left(\frac{\partial \mathcal{L}}{\partial y} - \frac{d}{dt} \frac{\partial \mathcal{L}}{\partial \dot{y}} \right) h = 0$$

Using that $h(a) = h(b) = 0$, the boundary terms vanish and using the fundamental lemma of calculus of variations, we obtain the differential equation

$$\frac{\partial \mathcal{L}}{\partial y} - \frac{d}{dt} \left(\frac{\partial \mathcal{L}}{\partial \dot{y}} \right) = 0. \tag{2.3}$$

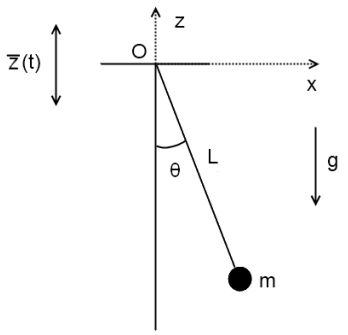

FIGURE 2.1: A schematic diagram of a pendulum with vertical motion $\bar{z}(t)$ of the pivot

which is the Euler-Lagrange equation of the system.

This approach will be used to find the equations of motion of the pendulum formulations considered.

2.2 Reference model: The classic pendulum

We will first seek to find the equations of motion of a classic planar pendulum (with rigid, non-stretchable string) attached to a support subjected to a prescribed vertical motion $\bar{z}(t)$ of the pivot point, see Fig. 2.1.

We start with the geometric description for accessible positions of the pendulum mass,

$$x(t) = L\sin\theta(t), \qquad z(t) = \bar{z}(t) - L\cos\theta(t)\,, \tag{2.4}$$

where L is the length of the pendulum and the reference frame is stationary.

The kinetic and gravitational potential energy of the system are defined as

$$T = \frac{1}{2}m(\dot{x}^2 + \dot{z}^2), \qquad U = mgz\,,$$

where m is the mass of the pendulum.

We will use Hamilton's principle to formulate the governing equations for the system [9], in terms of the Euler-Lagrange equations [11]:

$$\frac{\partial \mathcal{L}}{\partial u} - \frac{d}{dt}\left(\frac{\partial \mathcal{L}}{\partial \dot{u}}\right) = \frac{\partial F}{\partial \dot{u}}\,, \tag{2.5}$$

where $u(t)$ represents the state of the system and F is a Rayleigh dissipation function. This function describes damping terms in the equation of motion, which account for friction and other non-conservative effects might exist in the system.

In our case, the Lagrangian takes the form

$$\mathcal{L} = T - U = \frac{1}{2}m(L^2\dot{\theta}^2 + \dot{\bar{z}}^2 + 2L\dot{\theta}\dot{\bar{z}}\sin\theta) - mg\bar{z} + mgL\cos\theta\,, \tag{2.6}$$

and the dissipation function is $F = \frac{\beta}{2}|\boldsymbol{v}|^2$, where $\boldsymbol{v}$ is the velocity and $|\boldsymbol{v}|^2 = \dot{x}^2 + \dot{z}^2$.

Now we can proceed to finding $\frac{\partial \mathcal{L}}{\partial \theta}$ and $\frac{\partial \mathcal{L}}{\partial \dot{\theta}}$ and plugging them in (2.5) yields the equation of motion for θ:

$$\ddot{\theta} = -\frac{g + \ddot{\bar{z}}}{L}\sin\theta - \frac{\beta}{m}\dot{\theta} - \frac{\beta}{mL}\dot{\bar{z}}\sin\theta\,. \tag{2.7}$$

The classic pendulum system given by equation (2.7) will be used as a comparison to check the behaviors produced by the other models.

If we consider

$$\bar{z}(t) = A\cos(\omega t)\,, \tag{2.8}$$

and small damping β, then we can analyze the stability of the solution of equation (2.7). Different amplitudes A of the vertical forcing will produce qualitatively different solutions. The equations are solved numerically using the fourth order Runge-Kutta method [13]. Fig. 2.2 shows the phase plane for a periodic and a chaotic solution respectively. A few values of the parameter A (we will note that these values correspond to spikes to 0 in the Lyapunov exponent plot in Fig. 2.4) result in more complicated oscillations in the phase planes which are part of a series of bifurcations between periodic and chaotic solutions. An example is given in Fig.

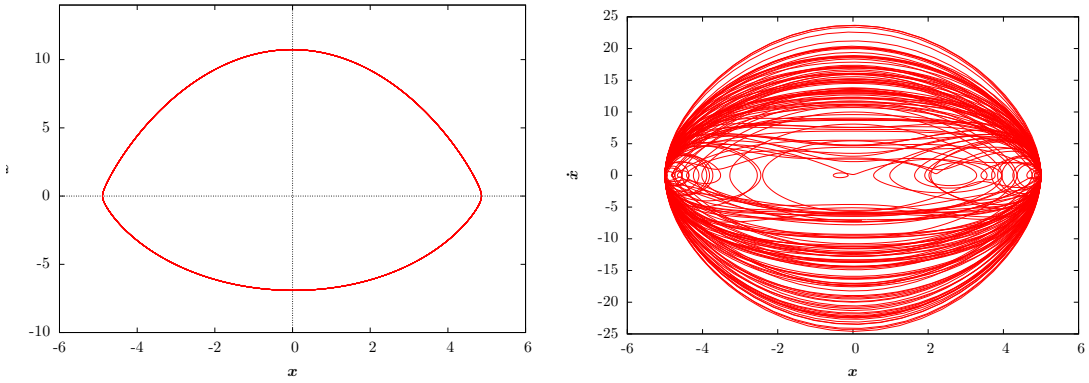

FIGURE 2.2: Phase planes of x vs. $\dot{x}$ for the forced damped pendulum for amplitude $A = 4\,\mathrm{m}$ (periodic oscillation), respectively $A = 11\,\mathrm{m}$ (chaotic motion) using equation (2.7). Parameter values used are $L = 5\,\mathrm{m}$, $g = 9.8\,\mathrm{m/s^2}$, $\omega = 0.9\sqrt{g/L}\,\mathrm{s}^{-1}$ and damping $\beta = 0.01\,\mathrm{kg/s}$.

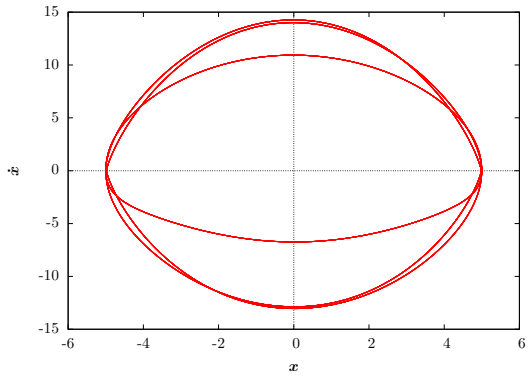

FIGURE 2.3: Phase plane of x vs. $\dot{x}$ for the forced damped pendulum for amplitude $A = 8.35$ showing oscillations using equation (2.7). Parameter values used are $L = 5$, $g = 9.8$, $\omega = 0.9\sqrt{g/L}$ and damping $\beta = 0.01$.

2.3 for $A = 8.35$. These behaviors hold systematically for most initial conditions the system can be started on and seem to depend on the forcing parameter value. We thus vary the forcing amplitude A and fix the other parameters to typical values, such as small damping β. A more thorough study of these equations of motion could take into account dependence on other parameter values.

Considering equation (2.7) with no damping ($\beta = 0$) and external forcing $\bar{z}$ as in

equation (2.8) yields

$$\ddot{\theta} + \left(\frac{g}{L} - \frac{A\omega^2}{L} \cos \omega t \right) \sin \theta = 0 \, .$$

By linearizing this equation for small angles, we obtain:

$$\ddot{\theta} + \left(\frac{g}{L} - \frac{A\omega^2}{L} \cos \omega t \right) \theta = 0 \, , \tag{2.9}$$

which is the linear Mathieu equation with the term $-\frac{A\omega^2}{L} \cos \omega t$ serving as a parametric excitation of the system. The Mathieu equation is actually closely related to the phenomenon of parametric resonance which occurs in the mechanical systems where a system is parametrically excited and oscillates at a resonant frequency [7].

2.3 Lyapunov exponents

Lyapunov exponents are a way of qualitatively and quantitatively characterizing systems' dynamical behavior. Lyapunov exponents determine a system's exponential divergence or convergence of nearby orbits in phase space. This is a way of showing sensitive dependence on initial conditions, meaning that neighboring orbits separate exponentially fast [15] and that solution behavior is thus unpredictable. Having one or more positive Lyapunov exponents defines a system as being chaotic [15], [17].

It is therefore important to identify the largest Lyapunov exponent of a system. Consider the general ODE system

$$\frac{d\boldsymbol{u}}{dt} = \mathbf{f}(\boldsymbol{u}, t) \, . \tag{2.10}$$

In order to compute its largest Lyapunov exponent, we consider a trajectory in phase space, $\boldsymbol{u_0}(t)$, given by the nonlinear equations of the system (2.10) applied to some initial condition. If we consider another trajectory starting nearby, $\boldsymbol{u_1}(t)$, and set

$\Delta \boldsymbol{u} = \boldsymbol{u_0} - \boldsymbol{u_1}$, then the logarithm of this difference represents the rate of exponential divergence or convergence: $\sigma = \ln |\Delta \boldsymbol{u}|/\Delta t$. When the length of the vector between the reference trajectory and a trajectory starting nearby becomes large, we choose a new trajectory close to the reference trajectory and repeat the process on the next time interval. Given $[t_n, t_{n+1}]$ time intervals considered, the largest Lyapunov exponent is given by the average growth rates for all of the time intervals [17]:

$$\sigma_{\max} = \lim_{k \to \infty} \frac{1}{k} \sum_{k} \frac{1}{t_{k+1} - t_k} \ln \frac{|\Delta \boldsymbol{u}(t_{k+1})|}{|\Delta \boldsymbol{u}(t_k)|} \,. \tag{2.11}$$

The following sections describe some approaches given in the literature or adjusted for our purposes for determining either the full spectrum or the largest Lyapunov exponent of a system.

2.3.1 Wolf method [17]

In [17], Wolf suggests a method that uses a phase space and tangent space approach and that can be applied to determine the largest Lyapunov exponent of a system. A "fiducial" trajectory is obtained by applying the nonlinear equations of motion of the system on some initial conditions. Then we apply the linearized equations of motion of the same system on points infinitesimally close to the fiducial trajectory. The nonlinear equations are then integrated (using Runge-Kutta) for some post-transient initial conditions. At the same time, the linearized equations of motion are integrated for n different initial conditions which represent a system of n orthonormal vectors. To avoid further singularities and computer limitations, the Gram-Schimdt reorthonormalization (GSR) process will be applied repeatedly on this system of vectors [17].

If the initial orthonormal system is given by $\{\boldsymbol{v_1}, ..., \boldsymbol{v_n}\}$ the Gram-Schmidt process is applied to these vectors to derive a new orthonormal set $\{\boldsymbol{v_1}', ..., \boldsymbol{v_n}'\}$ in the

following way:

$$
\begin{aligned}
\boldsymbol{v_1}' &= \frac{\boldsymbol{v_1}}{||\boldsymbol{v_1}||}\,, \\
\boldsymbol{v_2}' &= \frac{\boldsymbol{v_2} - (\boldsymbol{v_2}, \boldsymbol{v_1}')\boldsymbol{v_1}'}{||\boldsymbol{v_2} - (\boldsymbol{v_2}, \boldsymbol{v_1}')\boldsymbol{v_1}'||}\,, \\
&\vdots \\
\boldsymbol{v_n}' &= \frac{\boldsymbol{v_n} - (\boldsymbol{v_n}, \boldsymbol{v}'_{\boldsymbol{n-1}})\boldsymbol{v}'_{\boldsymbol{n-1}} - ... - (\boldsymbol{v_n}, \boldsymbol{v}'_{\boldsymbol{1}})\boldsymbol{v}'_{\boldsymbol{1}}}{||\boldsymbol{v_n} - (\boldsymbol{v_n}, \boldsymbol{v}'_{\boldsymbol{n-1}})\boldsymbol{v}'_{\boldsymbol{n-1}} - \boldsymbol{...} - (\boldsymbol{v_n}, \boldsymbol{v}'_{\boldsymbol{1}})\boldsymbol{v}'_{\boldsymbol{1}}||}\,.
\end{aligned}
\tag{2.12a}
$$

We note that while an equation like (2.7) would only require $n = 2$ trajectories, other equations of motion require larger n, so that the methods proposed here apply to the general case. We also mention that most of our calculations of the largest Lyapunov exponent use the Wolf method unless otherwise noted.

2.3.2 Rugh method [2]

While the Wolf method gives convergence of Lyapunov exponents to literature values (for systems such as the Lorenz equations), Rugh proposes an improved method of computing the full or partial Lyapunov spectrum associated with a dynamical system given by differential equations [2]. The method described in this paper introduces a stability parameter β and expands the system with an orthonormal k-dimensional system of vectors and a Lyapunov vector such that the system is continuously Gram-Schmidt orthonormalized (k is the number of Lyapunov exponents that the method will output). Therefore, the Gram-Schimdt reorthonormalization need not be performed anymore in the algorithm.

We let $k = n$ and the system of n orthonormal vectors be denoted by $\{\boldsymbol{e_1}(t), ..., \boldsymbol{e_n}(t)\}$ where $(\boldsymbol{e_i}, \boldsymbol{e_j}) = \delta_{ij}$ $1 \leqslant i, j, \leqslant n$ with $(\cdot, \cdot)$ the inner product. The Jacobian matrix of the system's differential equations will be denoted by J. The method introduces

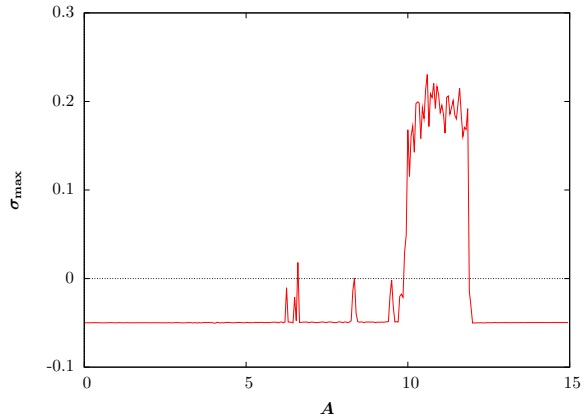

FIGURE 2.4: Parameter dependence of the largest Lyapunov exponent for a range of forcing amplitudes for the forced damped pendulum using the method in [17]. Parameter values used are $L = 5.0$, $g = 9.8$, $\omega = 0.9\sqrt{g/L}$, $\beta = 0.01$.

the matrix elements

$$J_{lm} = (\boldsymbol{e_l}, J\boldsymbol{e_m})$$

and the stabilized matrix elements

$$L_{mm} = J_{mm} + \beta((\boldsymbol{e_m}, \boldsymbol{e_m}) - 1)\,, \qquad L_{lm} = J_{lm} + J_{ml} + 2\beta(\boldsymbol{e_l}, \boldsymbol{e_m})\,,$$

where β is the stability parameter mentioned above. The system is also expanded with the Lyapunov vector $\boldsymbol{\Lambda} = \{\Lambda_1(t), ..., \Lambda_n(t)\}$.

The extended dynamical system that needs to be integrated now is, from [2]:

$$\dot{x} = v(x)\,, \tag{2.13a}$$

$$\dot{\boldsymbol{e}}_{\boldsymbol{m}} = J\boldsymbol{e_m} - \sum_{l \leqslant m} \boldsymbol{e_l} L_{lm}\,, \tag{2.13b}$$

$$\dot{\Lambda}_m = J_{mm}\,, \tag{2.13c}$$

for $m = 1, ..., n$.

According to [2], if we choose a stability parameter such that $\beta > -\lambda_k$, then the n Lyapunov exponents can be derived by the formula

$$\lim_{t\to\infty} \frac{1}{t}\Lambda_m(t) = \lambda_m \tag{2.14}$$

for $m = 1, ..., n$. This method is thus applied to determine the complete set of Lyapunov exponents of a system.

2.3.3 Limit definition for largest Lyapunov exponent

The methods for determining the Lyapunov exponents outlined in [17] and [2] use linearized ODE's for u_1. These methods could be extended and applied to the system of DAE's (differential algebraic equations) to be later discussed in section 4 by using linearized DAE systems; however, this would require more work since the Wolf and Rugh methods were designed for ODE systems. In order to compute the exponential divergence or convergence of trajectories in such a situation, we write, for $[t_k, t_{k+1}]$ in a sequence of time intervals: $\Delta \boldsymbol{u}(t_{k+1}) = \Delta \boldsymbol{u}(t_k) e^{\sigma(t_{k+1}-t_k)}$. When $0.1 < \frac{|\Delta \boldsymbol{u}(t_{k+1})|}{|\Delta \boldsymbol{u}(t_k)|} < 10$ ceases to be satisfied, which means that the length of the vector between the two points has become too large or too small, the next time interval is considered: $[t_k, t_{k+1}]$ is reset with $k \to k+1$. The largest Lyapunov exponent is thus given by equation (2.11), rewritten here for reference:

$$\sigma_{\max} = \lim_{k \to \infty} \sum_k \frac{1}{k} \frac{1}{t_{k+1} - t_k} \ln \frac{|\Delta \boldsymbol{u}(t_{k+1})|}{|\Delta \boldsymbol{u}(t_k)|} .$$

It is worth noting that this method, just like the one proposed by Wolf, determines only the largest Lyapunov exponent of the system.

In Fig. 2.4 we plot the largest Lyapunov exponent of the system versus the amplitude of the vertical forcing. We note how different values of A correspond to a chaotic ($A = 12$) or periodic ($A = 1$) solution, and the phase planes in Fig. 2.2 correspond to intervals of stable ($A = 4$) and unstable ($A = 11$) amplitudes. Moreover, the spikes going close to 0 in Fig. 2.4 may correspond to periodic systems that are not chaotic, as shown in Fig. 2.3 for amplitude $A = 8.35$. The Lyapunov exponents will provide us with a way to compare different ways of modeling the

pendulum systems considered. We calculate the Lyapunov exponents of the systems using the method described by Wolf in [17], with the exception of Chapter 4 and Chapter 6, where the DAE system of equations requires the use of equation (2.11). We propose the conjecture that comparable models will be similar in their stability behavior and thus have similar Lyapunov exponents, $\sigma_{\max}(A)$.

3

The Spring Pendulum

The derivation of (2.7) started with the geometric constraint on the length of the pendulum imposed through equation (2.4). As we will see later, imposing the constraint of fixed length after writing the Euler-Lagrange equations of a system creates more mathematical challenges. But such an approach will nevertheless allow for generalizing the problem, so it is of value for our later analysis. As a comparison problem, we first consider the dynamics for a spring pendulum, where the pendulum length can vary. Such a model is considered in [5], though no external force is applied to the system in that case.

In this chapter, we derive the equations of motion in polar coordinates for the spring pendulum formulation of the forced classic pendulum (section 3.1). This approximation is further analyzed in section 3.2 for the unforced case and in section 3.3 for the forced case. In both cases, we consider small amplitude oscillations for angle θ and derive equations of motion for the simplified system, which are then compared to the classic pendulum from Chapter 1. In section 3.4, we consider the spring pendulum system with a very large spring constant and show that its equations

of motion reduce to equation (2.7) for the forced damped classic pendulum. Section 3.5 introduces the first formulation of the string pendulum using a spring pendulum with piecewise constant stiffness, which will be compared to the DAE formulation in Chapter 6.

3.1 The Spring pendulum with vertical forcing

The spring pendulum can be compared to the rigid pendulum model while avoiding the exact geometric constraint that comes with a differential algebraic equation (DAE, to be considered later in Section 4). This system is also called a general "elastic pendulum" in [14].

The spring pendulum is a physical system with a mass connected to a spring so that the motion that results has characteristics of a simple pendulum as well as a spring. The spring is restricted to lie in a straight line, which can be achieved by wrapping the spring around a rigid massless rod [10]. We will consider such a spring pendulum with a large Hooke's law spring constant k which makes it moderately stiff, as well as a damping constant β which helps us control the stretching oscillation of the spring. We consider a pendulum made up of a spring with mass m on the end and let the angle it makes with the vertical be denoted by $\theta(t)$. The pendulum length $\tilde{L} = L - \frac{mg}{k}$ is selected so that the equilibrium length at $\theta = 0$ is L (see Fig. 3.1). The spring will thus have length $L + r(t)$ at time t.

As before, the spring pendulum in 2 dimensions has an imposed vertical forcing which represents a motion of the pendulum pivot point, $\bar{z}$ acting on it vertically. The results obtained will be compared against the behavior determined in equation (2.7).

The Lagrangian is

$$\mathcal{L} = T - U = \frac{1}{2}m(\dot{x}^2 + \dot{z}^2) - \left[mgz + \frac{1}{2}k\left(r + \frac{mg}{k}\right)^2\right], \tag{3.1}$$

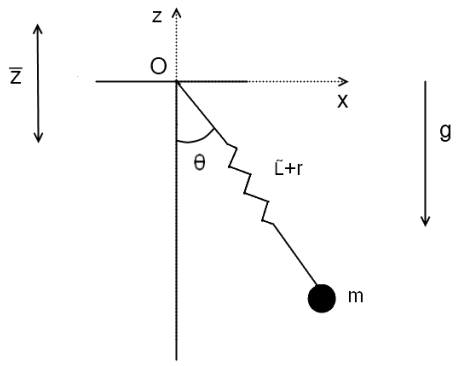

FIGURE 3.1: This figure provides a schematic diagram of a spring pendulum with un-stretched length $\tilde{L}$, equilibrium length L and stretch r, making an angle θ with the vertical

with x and z defined in this case as

$$x = (L + r)\sin\theta\,, \qquad z = \bar{z} - (L + r)\cos\theta\,. \tag{3.2}$$

Now we can apply the Euler-Lagrange equations with respect to r and θ. We again consider a Rayleigh dissipation function of the form $F = \beta|\boldsymbol{v}|^2/2$. The Euler-Lagrange equations are:

$$\ddot{r} = \ddot{\bar{z}}\cos\theta + (L + r)\,\dot{\theta}^2 + g\cos\theta - \frac{kr}{m} - g - \frac{\beta}{m}\dot{r} + \frac{\beta\dot{\bar{z}}}{m}\cos\theta\,, \tag{3.3a}$$

$$\ddot{\theta} = -\frac{g + \ddot{\bar{z}}}{L + r}\sin\theta - \frac{2}{L + r}\dot{r}\dot{\theta} - \frac{\beta}{m}\dot{\theta} - \frac{\beta\dot{\bar{z}}}{m(L + r)}\sin\theta\,. \tag{3.3b}$$

In Fig. 3.2 we plot the largest Lyapunov exponent of the spring pendulum system versus the amplitude of the vertical forcing. We note that, for smaller values of k such as $k = 250$ or $k = 500$, the Lyapunov exponent evolution is shifted to the right when compared to Fig. 2.4 and shows sharp drops, while for $k \to \infty$ the evolution matches very well that of Fig. 2.4. The largest Lyapunov exponent of the classic pendulum is plotted on the same graph and shows that this system has some higher values of the Lyapunov exponent for certain amplitudes A when compared to the

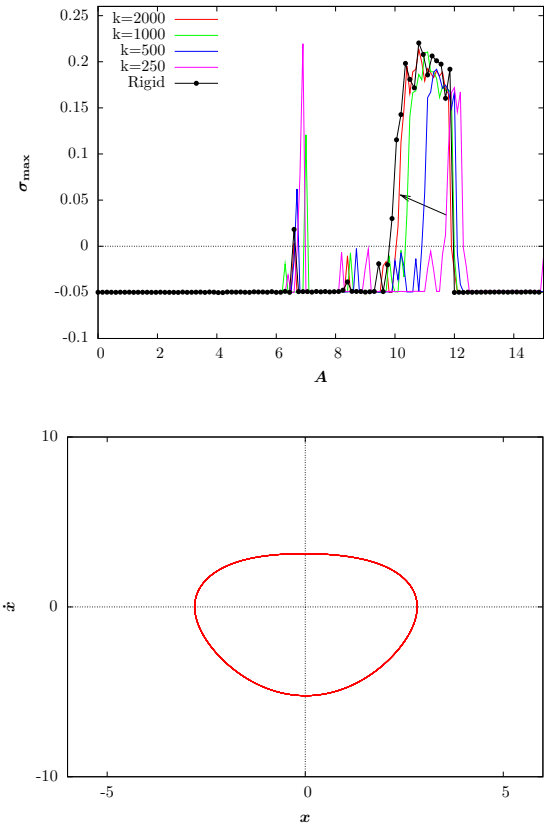

FIGURE 3.2: This figure for the forced damped spring pendulum shows (a) The progression of the largest Lyapunov exponent for amplitude A ranging from 0 to 15 at different spring constants k (using the Wolf method) and (b) A phase plane of x vs. $\dot{x}$ at stable forcing amplitude $A = 4$. Parameter values used are $\tilde{L} = 5$, $g = 9.8$, $\omega = 0.9\sqrt{g/\tilde{L}}$, $\beta = 0.01$ and $k = 1000$.

spring pendulum. Moreover, the ranges of chaotic behavior are slightly larger for the classic pendulum. However, Fig. 3.2 shows an overall very good match between the Lyapunov exponents of the classic and spring pendulums, which verifies our expectation that the Lyapunov exponent evolution of the two modeling methods should be similar. Fig. 3.2 also shows a phase plane for $A = 4$ that yields stable, periodic behavior as in the case of the forced damped pendulum in Fig. 2.2, in spite of the slightly different shape of the orbit.

3.2 Perturbation analysis of unforced case

We can explore the comparison of the spring pendulum to the classic pendulum more carefully by doing a perturbation analysis of the spring pendulum system. The analysis will be performed on the unforced case ($\bar{z} = 0$) of the spring pendulum, which yields the system of equations:

$$\ddot{r} = (L + r)\dot{\theta}^2 + g\cos\theta - \frac{k}{m}\left(r + \frac{mg}{k}\right) - \frac{\beta}{m}\dot{r} \tag{3.4a}$$

$$\ddot{\theta} = -\frac{g\sin\theta}{L + r} - \frac{2\dot{r}\dot{\theta}}{L + r} - \frac{\beta}{m}\dot{\theta} \tag{3.4b}$$

$$\theta(0) = \theta_0 \qquad \dot{\theta}(0) = 0 \qquad r(0) = 0 \qquad \dot{r}(0) = 0\,. \tag{3.4c}$$

We note that in this section we consider the total stretching of the spring ($r \to r + \frac{mg}{k}$), as opposed to considering it relative to the extension due to gravity at rest ($\frac{mg}{k}$). We will consider the case of small amplitude oscillations and define our asymptotic parameter as the initial angular position, $0 < (\epsilon = \theta(0)) \ll 1$. We write the expansions

$$\theta \approx \epsilon\theta_1(t) + \epsilon^2\theta_2(t) + \ldots\,, \qquad r \approx r_0 + \delta r_1(t) + \delta^2 r_2(t) + \ldots\,, \tag{3.5}$$

where $0 < \delta \ll 1$ is another small parameter whose relation to ϵ will be determined.

We seek a distinguished limit in order to determine this relationship between δ and ϵ. It should be mentioned that, in the absence of a distinguished limit, the derived equations of motion will not show the full $r - \theta$ coupling and will give a less accurate prediction of the dynamics.

We now expand equation (3.4a) to the next order and proceed with equation (3.4b) in order to find the behavior in terms of r_1 and θ_1:

$$\epsilon\ddot{\theta}_1 = -\frac{g}{L+\delta r_1}\sin\epsilon\theta_1 - \frac{2\delta\dot{r_1}\epsilon\dot{\theta}_1}{L+\delta r_1} - \frac{\beta}{m}\epsilon\dot{\theta}_1\,. \tag{3.6}$$

By using that $\sin(\epsilon\theta_1) \sim \epsilon\theta_1$, $\delta r_1 \ll 1$ and setting the ϵ^1 order terms equal, it follows that the equation of motion for θ_1 is:

$$\ddot{\theta}_1 = -\frac{g}{L}\theta_1 - \frac{\beta}{m}\dot{\theta}_1\,. \tag{3.7}$$

Similarly from (3.4a), we obtain:

$$\delta\ddot{r_1} = (L+\delta r_1)\,\epsilon^2\dot{\theta}_1^2 + g\left(1 - \frac{\epsilon^2\theta_1^2}{2}\right) - \frac{k}{m}\left(\delta r_1 + \frac{mg}{k}\right) - \frac{\beta}{m}\delta\dot{r_1}\,,$$

where we used the first two terms in the Taylor expansion of $\cos(\epsilon\theta_1) \sim 1 - \frac{\epsilon^2\theta_1^2}{2}$. This further reduces to

$$\delta\ddot{r_1} = \delta\left(\epsilon^2 r_1\dot{\theta_1}^2 - \frac{k}{m}r_1 - \frac{\beta}{m}\dot{r_1}\right) - \frac{g\epsilon^2\theta_1^2}{2} + \epsilon^2 L\dot{\theta_1}^2\,.$$

The term which has a factor of ϵ^2 inside the first parentheses can be ignored since it is much smaller than the others. Thus we obtain:

$$\delta\ddot{r_1} = \delta\left(-\frac{k}{m}r_1 - \frac{\beta}{m}\dot{r_1}\right) - \frac{g\epsilon^2\theta_1^2}{2} + \epsilon^2 L\dot{\theta_1}^2\,.$$

An appropriate choice of a relation between δ and ϵ is therefore $\delta = \epsilon^2$. Equating all $\mathcal{O}(\epsilon^2)$ terms gives us the equation of motion for r_1:

$$\ddot{r}_1 = -\frac{k}{m}r_1 - \frac{\beta}{m}\dot{r}_1 - \frac{g\theta_1^2}{2} + L\dot{\theta}_1^2\,. \tag{3.8}$$

A simulation which solves equations (3.7) and (3.8) is showed in figure 3.3 for r and θ. We note that the behavior coming from the perturbation analysis agrees very well

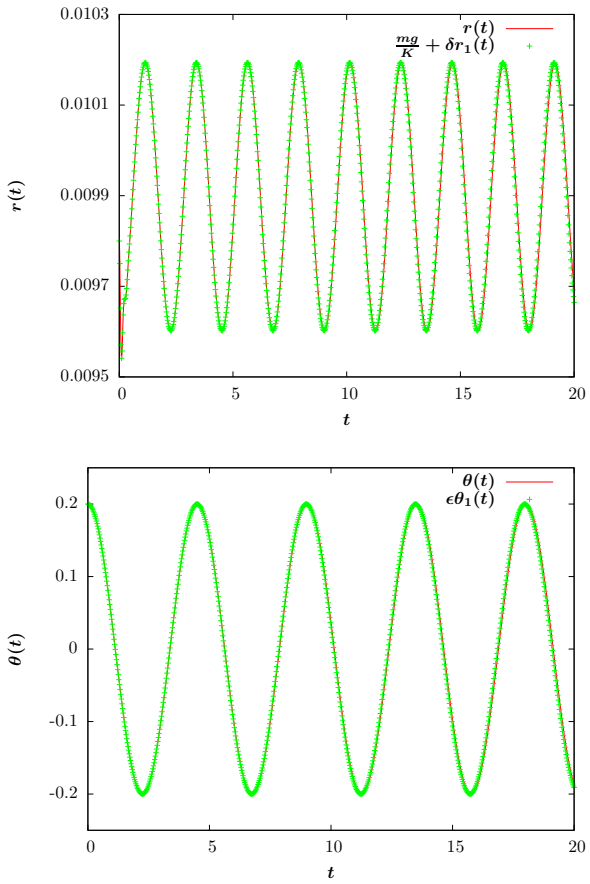

FIGURE 3.3: Comparison of the behavior given by the numerical simulation (points) and perturbation analysis (curves) for $r(t)$ and $\theta(t)$ respectively. Parameter values used are $\tilde{L} = 5$, $k = 1000$, $\beta = 20$, $m = 1$ and $\epsilon = 0.2$.

with the one generated by the original spring pendulum simulation, as shown in Fig. 3.3.

It is worth mentioning that the system of equations (3.7) and (3.8) is nonlinear, but can in fact be solved analytically, which provides a good check for the numerical simulation based on these equations.

3.3 Perturbation analysis of forced case

For the case of a non-trivial forcing $\bar{z}$, we again consider the case of small amplitude oscillations and define our asymptotic parameter as the initial angular position,

$\theta(0) = \epsilon \ll 1$. We write the expansions

$$\theta \sim \epsilon\theta_1(t) + \epsilon^2\theta_2(t) + \dots, \qquad r \sim r_0(t) + \epsilon r_1(t) + \epsilon^2 r_2(t) + \epsilon^3 r_3(t) + \dots. \tag{3.9}$$

It is useful to switch to looking at the stretching of the spring relative to the amount of gravity that occurs when the pendulum is hanging down with no forcing ($\frac{mg}{k}$). Thus, in this section the problem can be written in the form of equations (3.3), which we are rewriting here for reference.

$$\ddot{r} = \ddot{\bar{z}}\cos\theta + (L+r)\,\dot{\theta}^2 + g\cos\theta - \frac{k}{m}\left(r + \frac{mg}{k}\right) - \frac{\beta}{m}\dot{r} + \frac{\beta\dot{\bar{z}}}{m}\cos\theta\,,$$

$$\ddot{\theta} = -\frac{g + \ddot{\bar{z}}}{L+r}\sin\theta - \frac{2}{L+r}\dot{r}\dot{\theta} - \frac{\beta}{m}\dot{\theta} - \frac{\beta\dot{\bar{z}}}{m(L+r)}\sin\theta\,.$$

We use the above expansions in equation (3.10a) and since for $\epsilon \to 0$, $\cos\theta \sim 1 - \frac{\epsilon^2\theta_1^2}{2}$, the $\mathcal{O}(1)$ terms yield the equation for r_0:

$$\ddot{r}_0 + \frac{\beta}{m}\dot{r}_0 + \frac{k}{m}r_0 = \ddot{\bar{z}} + \frac{\beta}{m}\dot{\bar{z}}\,. \tag{3.11}$$

Equation (3.11) can be solved for our choice of external forcing given in (2.8). With initial conditions $r(0) = 0$, $\dot{r}(0) = 0$, the solution of equation (3.11) is:

$$r_0(t) = -\alpha_1 e^{-\frac{\beta}{2m}t}\cos(\Delta t) - \frac{\alpha_2\omega + \alpha_1\beta/(2m)}{\Delta}e^{-\frac{\beta}{2m}t}\sin(\Delta t) + \alpha_1\cos\omega t + \alpha_2\sin\omega t\,, \tag{3.12}$$

where $\alpha_1 = A\omega^2\frac{(\omega m)^2 - km + \beta^2}{(\beta\omega)^2 + (k-\omega m)^2}$, $\alpha_2 = -\frac{(\beta A\omega k}{(\beta\omega)^2 + (k-\omega m)^2}$ and $\Delta = \frac{\sqrt{\beta^2 - 4mk}}{2m}$.

We can see that equation (3.11) describes a damped, non-resonant linear oscillator. This means that, for large spring constant k, r_0 will be following the forcing

given by $\bar{z}$ and coming from the last two terms of equation (3.12) (the particular solution).

3.4 The case of large spring constant k

Now we consider equations (3.3) in the limit of a very large spring constant $k = \frac{1}{\epsilon}$, $\epsilon \to 0$ and small length perturbations $r = \epsilon\tilde{r}$. In (3.3a), this yields:

$$\epsilon\ddot{\tilde{r}} = \ddot{\bar{z}}\cos\theta + (L + \epsilon\tilde{r})\dot{\theta}^2 + g\cos\theta - g - \frac{\tilde{r}}{m} - \frac{\beta}{m}\epsilon\tilde{r} + \frac{\beta}{m}\dot{\bar{z}}\cos\theta$$

Using the expansion $\tilde{r} \sim \tilde{r}_0(t) + \epsilon\tilde{r}_1(t) + \epsilon^2\tilde{r}_2(t) + ...$, the $\mathcal{O}(1)$ terms give the following equation for $\tilde{r}_0$:

$$\tilde{r}_0 = mg(\cos\theta - 1) + m\ddot{\bar{z}}\cos\theta + mL\dot{\theta}^2 + \beta\dot{\bar{z}}\cos\theta\,. \tag{3.13}$$

If we assume that $\dot{\theta}$ is bounded (and thus $\dot{\theta}^2$ is bounded), then the equation for $\tilde{r}_0$ is also bounded. The same limits in (3.3b) give the equation:

$$\ddot{\theta} = -\frac{g + \ddot{\bar{z}}}{L + \epsilon\tilde{r}}\sin\theta - \frac{2}{L + \epsilon\tilde{r}}\epsilon\dot{\tilde{r}}\dot{\theta} - \frac{\beta}{m}\dot{\theta} - \frac{\beta\dot{\bar{z}}}{m(L + \epsilon\tilde{r})}\sin\theta\,. \tag{3.14}$$

Taking equation (3.14) in the limit $\epsilon \to 0$, we note that the term $L + \epsilon\tilde{r}$ in the denominator becomes L and the second term on the right hand side is $\mathcal{O}(\epsilon)$ and thus can be ignored to leading order. Therefore we conclude that in the limit $k \to \infty$ and $r = \epsilon\tilde{r}$ equations (3.3) are reduced to the equation for the forced damped pendulum (2.7).

The spring pendulum approach for modeling the rigid pendulum is thus appropriate for large spring constants k.

3.5 Spring pendulum with piecewise constant stiffness

So far we have considered a spring pendulum with a large spring constant so that it behaves similarly to the classic pendulum resisting stretching and compression. In switching to the string pendulum that can become slack under a vertical forcing $\bar{z}(t)$, the model of the spring pendulum needs to be adapted to model such slack states.

We thus consider the spring pendulum with piecewise constant stiffness, characterized by different spring constants k_1 and k_2 depending on whether the spring is extending or compressing relative to the fixed, original length of the string [6]. If k_1 is the constant associated with extension $r > 0$, this parameter should maintain a high value to prevent the pendulum from extending beyond its length L. If k_2 corresponds to compression $r < 0$, than this value should be relatively small to allow for some flexibility and low resistance to compression. Numerical simulation of the equations of motion suggested that $k_1 = 1000$ and $k_2 = 0.01$ are sufficiently high and respectively low values for these constants.

The equations of motion will be analogous to equations (3.3a) and (3.3b), but will include a condition that checks whether the pendulum is compressed or extended. This is controlled by the variable r:

$$\kappa(r) = \begin{cases} k_1 & \text{if } r \geqslant 0\,, \\ k_2 & \text{if } r < 0\,. \end{cases} \tag{3.15a}$$

$$\ddot{r} = \ddot{\bar{z}}\cos\theta + (L+r)\dot{\theta}^2 + g\cos\theta - \frac{\kappa(r)r}{m} - g - \frac{\beta}{m}\dot{r} + \frac{\beta\dot{\bar{z}}}{m}\cos\theta\,. \tag{3.15b}$$

The equation of motion for θ is unchanged from equation (3.3b).

Fig. 3.4 provides a comparison of the spring pendulum with piecewise constant stiffness with the simple spring pendulum analyzed earlier in this section, as well as

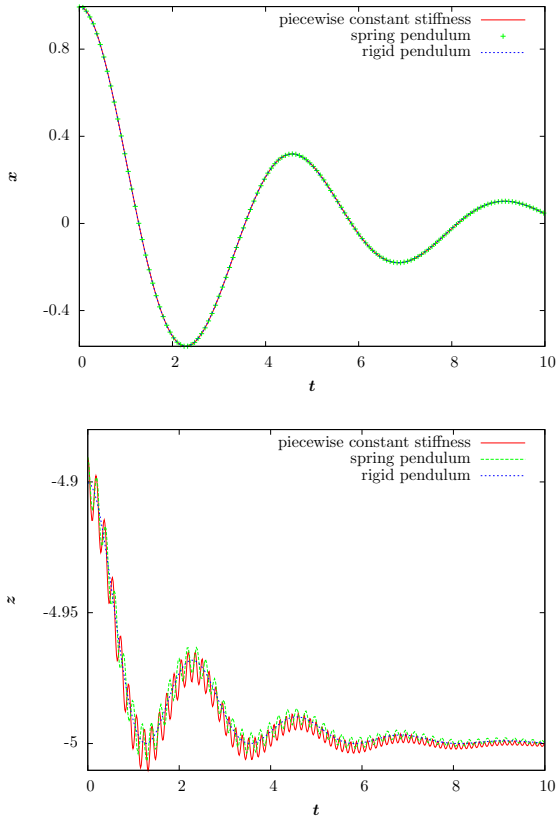

FIGURE 3.4: For small angle oscillations, this shows a good match of the time profiles for the motion of the spring pendulum with piecewise constant stiffness, the simple spring pendulum and the rigid pendulum. Parameter values used are $A = 0$, $L = 5$, $g = 9.8$, $\beta = 0.5$, $k_1 = 1000$, $k_2 = 0.01$ (for piecewise constant stiffnesses) and $k = 1000$ (for the simple spring pendulum).

the rigid pendulum in Chapter 2.2. We consider the unforced case with $\bar{z}(t) \equiv 0$ and note that the motions in the x direction match almost indistinguishably for small angle oscillations, while the z behaviors differ. We choose to compare the x, z directions as opposed to the r, θ ones because the DAE approach in section 4 also uses Cartesian coordinates. We note that the slow, damped oscillations in the z direction for the spring pendulum are due to the large value of the spring constant k, while the faster oscillations for the spring pendulum with piecewise constant stiffness are due to the large k_2 and very small k_1, which allows the string to have a lower resistance to compression.

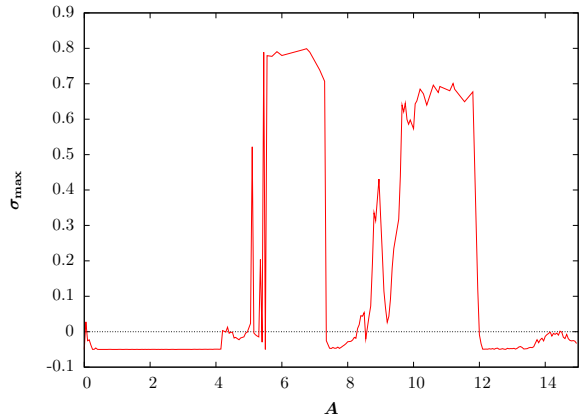

FIGURE 3.5: The dependence of the largest Lyapunov exponent for the spring pendulum with piecewise constant stiffness on amplitude A ranging from 0 to 15 (using Wolf's method). Parameter values used are $\omega = 0.9\sqrt{g/L}$, $\tilde{L} = 5 - r_0$, $g = 9.8$, damping $\beta = 0.1$ and $k_1 = 1000$, $k2 = 0.01$.

A Lyapunov exponent dependence on a range of amplitudes for the spring pendulum with piecewise constant stiffness is showed in Fig. 3.5. Since this corresponds to the largest Lyapunov exponents for a string pendulum, it cannot be compared with Fig. 2.4 and 3.2(a), which are formulations of the classic pendulum. We note that numerical problems can occur because of the expression of the problem in polar coordinates and due to the denominators $L + r$ in equation (3.3b). A comparison with Fig. **??**a) shows similar chaotic behavior in the range A = 10-12 and stable solutions for small amplitudes. However, Fig. 3.5 has another range of chaotic behaviors centered at amplitude $A = 6$. This difference might arise due to the slack behavior modeled for the spring pendulum with piecewise stiffness using the small coefficient of compression k_2.

The work in this section suggests that the string pendulum can be approximated with the model of a spring pendulum with piecewise constant stiffness, which allows for the string of the pendulum to become slack under some exterior forcing amplitudes. An analysis of the accuracy of this approximation is provided in Chapter 6. A comparison with the modeling method of the string pendulum introduced in

Chapter 4 will help identify the advantages and disadvantages of considering a spring pendulum with piecewise constant stiffness.

4

DAE re-formulation of the classic pendulum

In this Chapter, we formulate the classic pendulum system described by equation (2.7) using a differential-algebraic equation system (DAE), which is a system of ODE's to which we can apply the Euler-Lagrange method. In this case, the Lagrangian will include an extra term based on a geometric constraint with a Lagrange multiplier. The formulation given in Chapter 2.2 is the natural way of modeling the rigid pendulum, however it leads to numerical problems when adjusted for the pendulum that can go through slack states. In Chapter 5, this DAE method will be extended to consider the case of a flexible pendulum string.

Since we want to work in the stationary reference frame (and thus keep track of the vertical motion $z - \bar{z}$, which will prove useful when switching from taut to slack states), we will be working with x, z coordinates as opposed to the polar coordinates we used so far. In our case, the geometric condition is a rheonomic constraint [4] coming form the fact that the pendulum string is inextensible and thus restricts the motion of the mass:

$$f(\lambda) \equiv x(t,\lambda)^2 + (z(t,\lambda) - \bar{z}(t))^2 - L^2\,, \tag{4.1}$$

and we require that $f(\lambda) = 0$. The Lagrange multiplier $\lambda(t)$ may be interpreted as being related to the tension force in the string.

The Lagrangian $\mathcal{L} = \mathcal{L}(x, z, \lambda) = \mathcal{L}(\boldsymbol{u})$ becomes

$$\mathcal{L} = T - U = \frac{1}{2}m(\dot{x}^2 + \dot{z}^2) - mgz - \lambda(x^2 + (z - \bar{z})^2 - L^2)\,.$$

From the Euler-Lagrange equation (2.5) with respect to each variable in $\boldsymbol{u} = (x, z, \lambda)$ and the Rayleigh dissipation function, which is again taken to be of the form $F = \frac{\beta}{2}(\dot{x}^2 + \dot{z}^2)$, we can deduce

$$\ddot{x} = -\frac{2\lambda x}{m} - \beta\dot{x}\,, \tag{4.2a}$$

$$\ddot{z} = -g - \frac{2\lambda(z - \bar{z})}{m} - \beta\dot{z}\,, \tag{4.2b}$$

$$0 = x^2 + (z - \bar{z})^2 - L^2\,. \tag{4.2c}$$

In order to solve this system, at each time step in a numerical simulation we need to determine λ so that (4.2c) is satisfied. We do this by evolving equations (4.2a) and (4.2b) and checking if condition (4.2c) is satisfied. If it is not, we adjust λ and redo the evolution of x and z. We adjust λ using Newton's method to converge to the $\lambda(t)$ value for each time step:

$$\lambda_{k+1} = \lambda_k - \frac{f(\lambda_k)}{f'(\lambda_k)}\,, \tag{4.3}$$

with f given by (4.1).

A method of computing the denominator in the above equation that is numerically more efficient is to differentiate the expression for f in terms of x and z as a function of λ. Thus, starting with $f(\lambda) = x(\lambda)^2 + (z(\lambda) - \bar{z})^2 - L^2$, we obtain $f'(\lambda) =$

$2x\frac{\partial x}{\partial \lambda} + 2(z-\bar{z})\frac{\partial z}{\partial \lambda}$. We will call the derivatives of x and z with respect to λ as η and ξ, then it follows that $f'(\lambda) = 2x\eta + 2(z-\bar{z})\xi$.

Therefore, we have two extra ODE's coming from taking derivatives with respect to λ of the original equations (4.2a), (4.2b). The system under consideration becomes:

$$\ddot{x} = -\frac{2\lambda x}{m} - \beta\dot{x}\,, \tag{4.4a}$$

$$\ddot{z} = -g - \frac{2\lambda(z-\bar{z})}{m} - \beta\dot{z}\,, \tag{4.4b}$$

$$\ddot{\eta} = -\frac{2}{m}x - \frac{2\lambda}{m}\eta - \beta\dot{\eta}\,, \tag{4.4c}$$

$$\ddot{\xi} = -\frac{2}{m}(z-\bar{z}) - \frac{2\lambda}{m}\xi - \beta\dot{\xi}\,, \tag{4.4d}$$

$$0 = x^2 + (z-\bar{z})^2 - L^2\,. \tag{4.4e}$$

The initial conditions for x and z are unchanged, and $\eta = \dot{\eta} = 0$ and $\xi = \dot{\xi} = 0$ since we will compute λ independently on each time step.

Thus there is no ODE for the λ variable, but the value from the algorithm above is determined indirectly from x and z so that they satisfy (4.4e). Then once λ is known, equations (4.4a) and (4.4b) determine the evolution of $x(t)$ and $z(t)$.

The simulation based on the DAE system and Newton's method implies using equation (4.3) for a number of iterations for each time step. Six iterations suffice for convergence of Newton's method in this case, and the numerical scheme is first order accurate. Since the Runge-Kutta integration is called in each call of function f, the integration is performed several times for each time step. This is more complicated and takes more time than the simulation for the spring pendulum model, which involves using a simple Runge-Kutta integration applied to equations (3.3a) and (3.3b). However, the method presented in this section describes the string pendulum

system by definition and avoids the oscillations around the trajectories obtained in the spring pendulum model.

We note that the simulation described in Chapter 3 matches the simulation generated using the DAE formulation well. Moreover, Fig. 4.1 shows an evolution of the largest Lyapunov exponent of the system for a range of A's that matches closely the one for the classic and spring pendulums, see Fig. 2.4 and 3.2. The excellent agreement with Fig. 2.4 was expected since both the DAE formulation and the one in Chapter 2.2 describe the same physical system of a classical pendulum with non-stretchable and non-compressible string. This agreement over the whole parameter range shows that the method of determining the largest Lyapunov exponent of a system described by equation (2.11) at the end of Chapter 2.4 and used for the DAE formulation matches the methods in [17] and [2] used for the classic and spring pendulum systems. The differences in the number and amplitude of spikes to 0 in the two Lyapunov exponent plots should be noted and are due to the different numerical approaches used in computing the exponents. While [17] and [2] use the linearized equations for the nearby trajectory $\boldsymbol{u_1}$ and give all the Lyapunov exponents of the system, the method applied to the DAE system uses only two nearby trajectories on the full system and only determines the largest Lyapunov exponent $\sigma_{\max}$.

We will now use this DAE formulation to set up the taut-slack problem for the string pendulum in the next chapter.

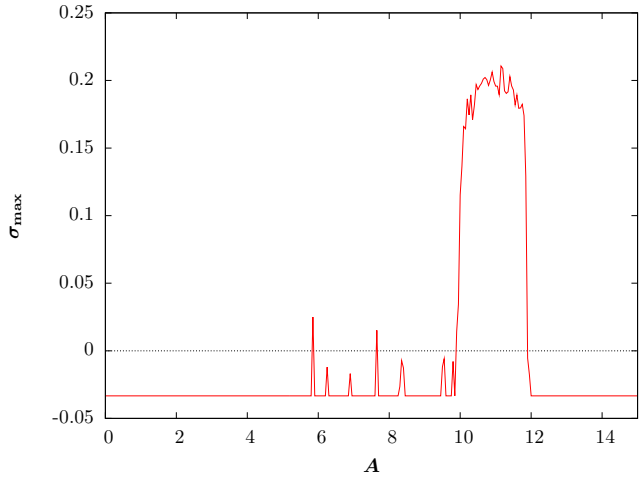

FIGURE 4.1: Dependence of the largest Lyapunov exponent for the forced damped pendulum modeled using the DAE formulation on amplitude A ranging from 0 to 15 (using limit definition for σ_max method). Parameter values used are $L = 5$, $g = 9.8$, $\omega = 0.9\sqrt{g/L}$, $\beta = 0.01$.

5

The taut-slack pendulum

In this Chapter, we consider the possibility of the pendulum string becoming slack, i.e. $x^2 + (z - \bar{z})^2 < L^2$), in order to analyze the dynamics of the string pendulum. In Chapter 4 we proposed a re-formulation of the rigid pendulum problem with external forcing. We now explore how the behavior of the system changes when switching from a rigid rod of length L to a massless string of length L. The simulation of the slack pendulum will cause some challenges since it will need to take into account the fact that the pendulum string cannot stretch to a length bigger than L.

Some of these challenges include the limitations of the DAE formulation described in section 4. The DAE setup assumes that the problem's initial conditions satisfy the taut pendulum state, so any variation from this initial assumption can lead to unreasonable evolutions of the trajectories. For instance, if the pendulum string is slack or stretched out at the start of the simulation, there are no changes in the x direction however the z direction does not obey the taut pendulum state. In the case of starting in the taut pendulum state, but with velocities in the x and z directions creating a positive outward normal velocity, the DAE simulation trajectories match the evolution from the taut initial conditions.

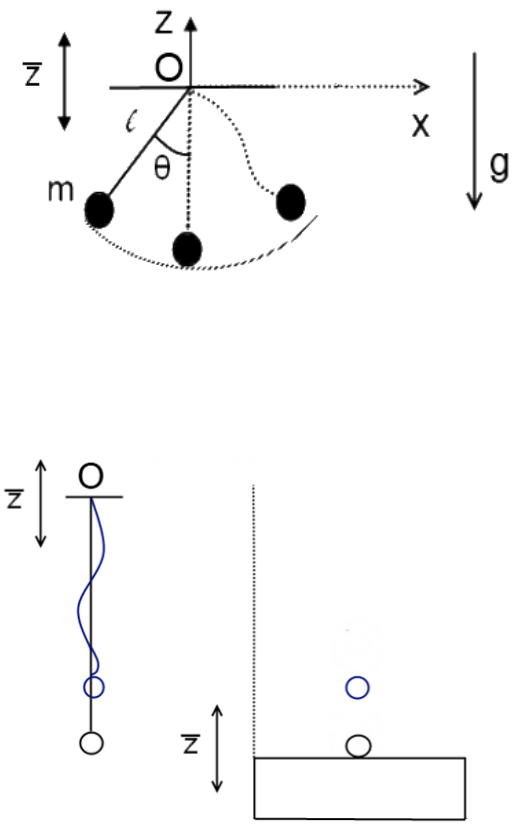

FIGURE 5.1: This figure shows (a) A schematic diagram of the string pendulum in both the taut and slack states and (b) A string pendulum under external forcing with no horizontal motion

We start by considering the string pendulum in 2D with point of attachment moving with a vertical motion $\bar{z}(t)$ as showed in Fig. 5.1(a). We note how the pendulum mass can be fully extended and constrained by the string length, but given enough velocity it can jump and follow a parabolic path until the string is extended again [5]. We will consider $\bar{z}$ to be a sinusoidal motion of the form of equation (2.8).

We need to differentiate between two situations, called the slack and taut states. When the pendulum is slack, $x^2 + (z - \bar{z})^2 < L^2$, where L is the length of the

pendulum, we would have the equations of motion:

$$\ddot{x} = -\frac{\beta}{m}\dot{x}\,, \qquad \ddot{z} = -g - \frac{\beta}{m}\dot{z}\,, \tag{5.1}$$

since the mass of the pendulum would just be in free fall and thus only affected by gravity and damping due to air resistance. We note that the above equations with the change of variables $x = (L+r)\sin\theta\,, z = \bar{z} - (L+r)\cos\theta$ yield equations (3.3) with the exception of the spring restoring force in the term $-\frac{k}{m}\left(r(t) + \frac{mg}{k}\right)$. This shows that the spring pendulum and taut-slack formulations are consistent.

The taut case will be in turn characterized by equations (4.4) and our main focus now is on switching between these dynamical states.

5.1 Switching conditions in absence of horizontal motion

A simulation using equations (4.4) for the taut case and equations (5.1) for the slack case fails to take into account the fact that the pendulum string cannot stretch for a length greater than L. In order to solve this problem, we first reduce it to an easier one, a one-dimensional problem for a particle that can only move in the z direction. There is no forcing in the x direction, and if $x(0) = 0$ then $x(t) \equiv 0$ for any t. We thus reduce the problem to the 1D case. The Lagrangian in this case is $\mathcal{L} = T - U = \frac{1}{2}m\dot{z}^2 - mgz$.

To gain insight into the solution to this problem, we identify the similarity between this situation and the one of the ball positioned on a sinusoidally-vibrating table, which also exhibits a switching behavior [3], see Fig. 5.1(b). Using the insight gained from this situation, the acceleration equation is

$$\ddot{z} = \begin{cases} \ddot{\bar{z}} - \beta\dot{z} & \text{if } z \leqslant \bar{z} - L \text{ and } (\dot{z} - \dot{\bar{z}})(z - \bar{z}) > 0, \\ -g - \beta\dot{z} & \text{else.} \end{cases} \tag{5.2}$$

We note that we should also take into account the fact that our Euler-Lagrange approach might be affected by the "corner conditions" imposed at times when the mass of the pendulum is going from slack to fully stretched and vice versa [11]. Based on the analogy between impacts of the ball bouncing off table and pendulum mass being constrained by a string, we write a corner condition relating the velocity immediately before and after impact (at time t_*). We use c to denote the coefficient of restitution and thus $c = 1$ for an elastic rebound (stretchy string), $0 < c < 1$ for a partially inelastic rebound and $c = 0$ for a completely inelastic impact (unstretchable string). The corner condition is given in the moving reference frame by:

$$\dot{z}(t_*^+) = -c\dot{z}(t_*^-)\,, \tag{5.3}$$

so that in the stationary reference frame we obtain $\dot{z}(t_*^+) = \dot{\bar{z}} - c\dot{z}(t_*^-)$.

5.2 Switching conditions for general motion

Now we are left with finding corner conditions for the case of the 2D pendulum. Our physical understanding of the system indicates that, in order for the no-stretch condition to be satisfied, we would need to check the velocity in the normal direction of the pendulum when it reaches a taut position. If the normal component of the velocity is greater than zero, than it needs to be zeroed in the code so that the simulation does not allow the string to go over its maximum length of L: $x^2 + (z - \bar{z})^2 = L^2$. A similar idea is introduced in [5], where the radial component of the velocity of the mass is zeroed when the string becomes taut in the case of a toy jumping pendulum.

The normal vector to the trajectory of the pendulum when it makes an angle θ with the vertical is $\boldsymbol{n} = (\cos\theta, \sin\theta)$, while the vector tangent to this trajectory is $\boldsymbol{t} = (\sin\theta, -\cos\theta)$.

We will denote by $\boldsymbol{v}^-$ the velocity of the string before reaching the taut position and by $\boldsymbol{v}^+$ the velocity right after this position. We will therefore have an equation of $\boldsymbol{v}^-$ in terms of $\boldsymbol{v}_n^-$ and $\boldsymbol{v}_t^-$ and an equation relating $\boldsymbol{v}^+$ to $\boldsymbol{v}_n^+$ and $\boldsymbol{v}_t^+$. We will try to find the values of the latter two velocities that correspond to out physical understanding of the system as described above. We also denote the norm of these vectors by: $v_n^- = ||\boldsymbol{v_n^-}||$ and $v_t^- = ||\boldsymbol{v_t^-}||$. We will consider the system in the moving reference frame in the following derivation.

We start with $\boldsymbol{v}^- = v_n^-\boldsymbol{n} + v_t^-\boldsymbol{t} = (\dot{x}, \dot{z})$. We can thus find $\boldsymbol{v}_n^-$ and $\boldsymbol{v}_t^-$ by finding the projection of $\boldsymbol{v}^-$ on the normal and tangential directions:

$$\boldsymbol{v}_n^- = (\dot{x}\cos\theta + \dot{z}\sin\theta)(\cos\theta, \sin\theta)\,, \qquad \boldsymbol{v}_t^- = (\dot{x}\sin\theta - \dot{z}\cos\theta)(\sin\theta, -\cos\theta)\,.$$

Similarly, one can obtain equations for the states following the taut position:

$$\boldsymbol{v}_n^+ = (\dot{x}^+\cos\theta + \dot{z}^+\sin\theta)(\cos\theta, \sin\theta)\,, \qquad \boldsymbol{v}_t^+ = (\dot{x}^+\sin\theta - \dot{z}^+\cos\theta)(\sin\theta, -\cos\theta)\,.$$

The relation between the two states is summarized as

$$\boldsymbol{v}_n^+ = -c\boldsymbol{v}_n^-\,, \qquad \boldsymbol{v}_t^+ = \boldsymbol{v}_t^-\,, \tag{5.4}$$

for c representing the coefficient of restitution.

We solve the system of equations (5.4) and obtain:

$$\dot{x}^+ = \dot{x}(\sin^2\theta - c\cos^2\theta) + \dot{z}(-\sin\theta\cos\theta - c\sin\theta\cos\theta)\,,$$

and

$$\dot{z}^+ = \dot{x}(-c\sin\theta\cos\theta - \sin\theta\cos\theta) + \dot{z}(\cos^2\theta - c\sin^2\theta)\,.$$

Using that $\sin\theta = \frac{z-\bar{z}}{L}$ and $\cos\theta = \frac{x}{L}$, as well as the assumption of inelastic collision $c = 0$, we can find the values for the velocities in the x and z directions:

$$\dot{x}^+ = \dot{x}\frac{(z-\bar{z})^2}{L^2} - (\dot{z}-\dot{\bar{z}})\frac{x(z-\bar{z})}{L^2}\,, \qquad \dot{z}^+ = \dot{\bar{z}} - \dot{x}\frac{x(z-\bar{z})}{L^2} + (\dot{z}-\dot{\bar{z}})\frac{x^2}{L^2}\,. \tag{5.5}$$

We can therefore summarize the switching between the taut and slack states of the string pendulum as follows:

1. If the string is taut ($x^2 + (z-\bar{z})^2 = L^2$) and stretching out ($x\dot{x} + (z-\bar{z})(\dot{z}-\dot{\bar{z}}) > 0$), then:
   (a) If the string was previously slack, apply equations (5.5) to determine the updated velocities and then use equations of motion (4.4).
   (b) If the string was previously taut, use equations of motion (4.4).
2. If the string is slack, then use equations of motion for free fall (5.1).

This algorithm will be used in the next chapter in order to perform numerical simulations of the taut-slack system and compare its behavior with that of the spring pendulum with piecewise constant stiffness formulation.

6

Comparison of the DAE and spring models of the taut/slack pendulum

In this Chapter, we compare the approximation given by the spring pendulum with piecewise constants stiffness against the model of a string pendulum that switches between the taut and slack positions using the conditions identified in Chapter 5.2. The spring pendulum formulation of the string pendulum system is described by equations (3.3b) and (3.15) in Chapter 3.5.

First, we note the x and z trajectories of motion for the taut-slack formulation in Fig. 6.3, which also indicates the times when the string pendulum is taut (green line above trajectory) and slack (green line below trajectory). For an amplitude of $A = 10$, the string pendulum thus goes through consecutive taut and slack states.

In order to compare these two models of the string pendulum, we first consider the case of no forcing ($A = 0$). The two approximations seem to match very well for the unforced case, as we can see from the evolution of the x and z trajectories in figure 6.1. Similarly, figure 6.2 shows the phase plane of the system (z vs. $\dot{z}$). The phase plane corresponding to the spring pendulum model seems to wrap around the

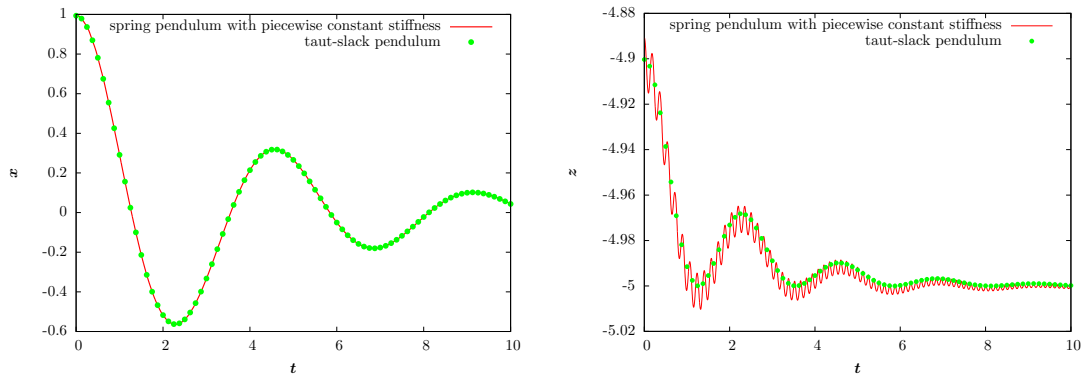

FIGURE 6.1: Comparison of time profiles for the motion in the x (left) and z (right) coordinates for the string pendulum modeled using the spring pendulum with piecewise constant stiffness and the taut-slack formulation. Parameter values used are $A = 0$, $L = 5$, $g = 9.8$, damping $\beta = 0.5$.

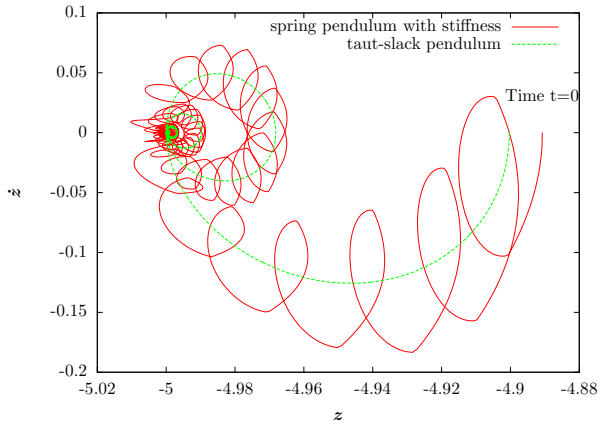

FIGURE 6.2: Phase plane (z vs. $\dot{z}$) for the spring pendulum with piecewise constant stiffness and the taut-slack formulation (same parameter values, $A = 0$)

one determined using the DAE model, which is explained by the fact that the spring pendulum is allowed to compress and stretch out.

We can observe the effects of increasing the forcing amplitude A in Fig. 6.4. We note that the x and z trajectories of the two models agree with the increase of amplitude, although the x time profiles are not in perfect agreement. The spring pendulum with piecewise constant stiffness provides a good, simple approximation of the forced string pendulum, but diverges slightly from the DAE model as the forcing amplitude increases. On the other hand, the DAE model behaves as expected but

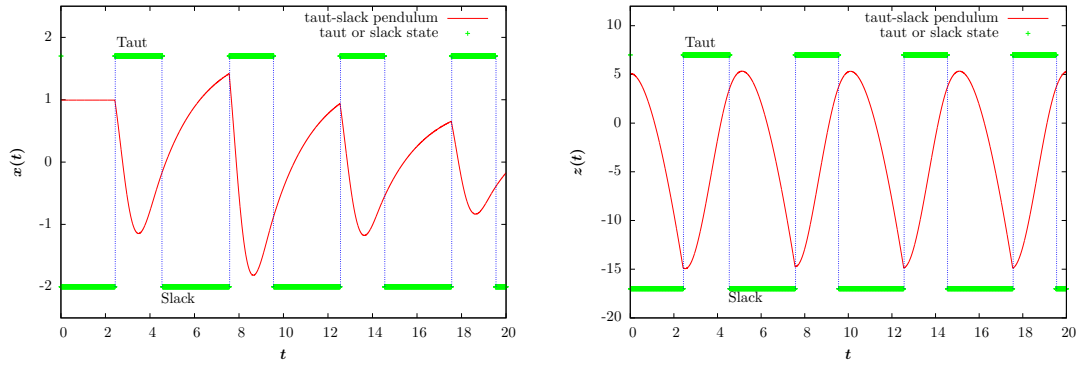

FIGURE 6.3: The time profiles in the x (left) and z (right) coordinates for the forced string pendulum modeled using the taut-slack formulation. Parameter values used are $A = 10$, $\omega = 0.9\sqrt{g/L}$, $L = 5$, $g = 9.8$, damping $\beta = 0.5$.

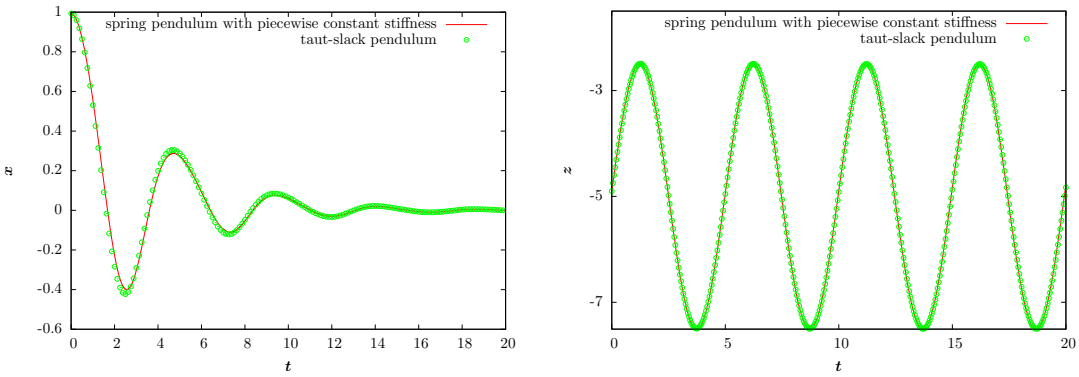

FIGURE 6.4: Time profiles in the x (left) and z (right) coordinates for the forced string pendulum modeled using the spring pendulum with piecewise constant stiffness and the DAE model. Parameter values used are $A = 2.5$, $\omega = 0.9\sqrt{g/L}$, $L = 5$, $g = 9.8$, damping $\beta = 0.5$.

requires a more complex algorithm and switching between two sets of equations of motion. The phase plane z vs. $\dot{z}$ for the same amplitude $A = 2.5$ is showed in Fig. 6.5, and we note the very good agreement between the planes and the stable periodic cycle of the behavior after the early transients have passed. This is an example of an amplitude value for which the solution converges to a steady solution.

We can also note that the two methods used in modeling the string pendulum are similar in the stability of the solutions. Fig. 3.5 in Chapter 3 shows a dependence of the largest Lyapunov exponent for the spring pendulum with piecewise constant

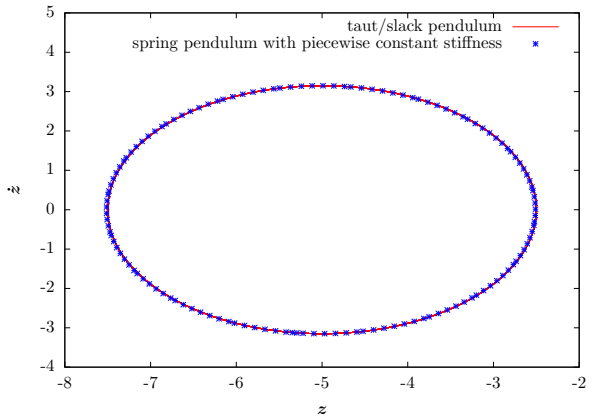

FIGURE 6.5: Phase plane (z vs. $\dot{z}$) for the spring pendulum with piecewise constant stiffness and the taut-slack formulation (same parameter values, $A = 2.5$)

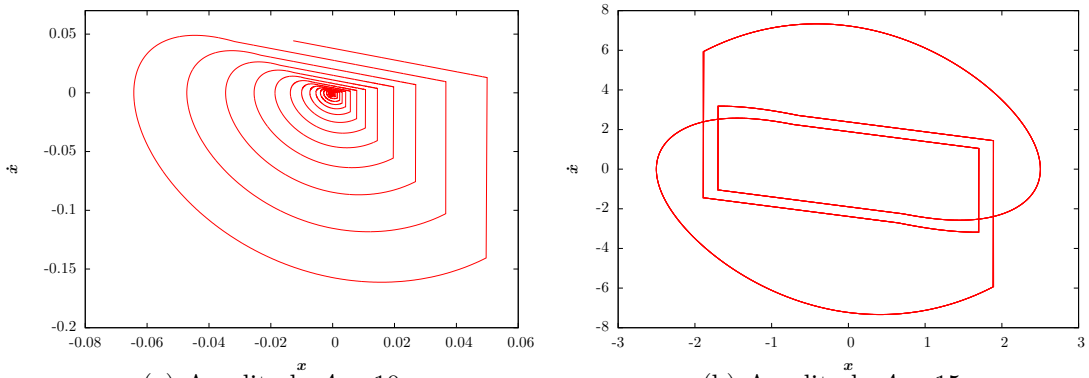

(a) Amplitude $A = 10$ (b) Amplitude $A = 15$

FIGURE 6.6: Phase planes x vs. $\dot{x}$ for the motion for the taut-slack string pendulum. Parameter values used are $\omega = 0.9\sqrt{g/L}$, $L = 5$, $g = 9.8$, damping $\beta = 0.5$.

stiffness on a range of amplitudes. Such a plot is difficult to produce for the case of the DAE modeling method, because of the resetting of velocities at times when the string pendulum might go from a slack to a taut case.

However, we can still observe the dynamics generated by this method through phase planes at different amplitudes. Fig. 6.6 shows the phase planes in the x component for the taut-slack formulation when amplitude $A = 10$ and $A = 15$, respectively. The first phase plane is an inward spiral because the oscillations in the x direction keep getting smaller even after earlier transients are gone, while

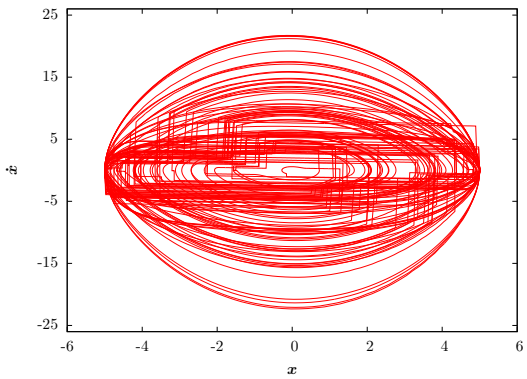

FIGURE 6.7: Phase plane (x vs. $\dot{x}$) for the taut-slack string pendulum. Parameter values used are $A = 11.0$, $\omega = 0.9\sqrt{g/L}$, $L = 5$, $g = 9.8$, damping $\beta = 0.5$.

the second is a periodic cycle, which matches our expectations from the Lyapunov exponents corresponding to these values in Fig. 3.5. These are cases in which the solutions approach steady solutions in the moving reference frame (with $x(t) \equiv 0$ and $z(t) \equiv \bar{z}(t)$). We note that for both of these amplitudes the string pendulum goes through both taut and slack states. An example of a chaotic solution for the taut-slack formulation of the string pendulum is given in figure 6.7 for amplitude $A = 11$.

7

Conclusions and further work

We have modeled the classic pendulum using both a spring pendulum and a differential algebraic system (DAE) approach. The string pendulum, which is not as well understood as the classic pendulum, was approximated using a spring pendulum with piecewise constant stiffness and a DAE system with switching between the taut and slack cases. These modeling methods proved to match very well, as proven by the time profiles and phase planes of the trajectories. Moreover, the dependence of the largest Lyapunov exponent of the system on parameter A denoting amplitude of the forcing shows that the stability behavior and dynamics of the approximations are also similar.

More work can be done in determining the Lyapunov exponents of the DAE formulation for the string pendulum. This would allow a complete comparison of this method with the spring with piecewise constant stiffness. An analysis of the stability of equations (A.12) would also be of interest in order to be able to describe the 3-dimensional system.

A more thorough study of the formulations' dependence on parameters would include holding forcing amplitude A fixed and changing the forcing frequency ω,

which could be used to study resonant responses. We note that the values of the length L and amplitude A considered here may be relevant for applications such as moored boats, but the dynamics for other motivations should be investigated for smaller values of these parameters. Another possibility for future work is looking for multiple stable states by starting from different initial conditions at the same system parameters. Alternatively, the the system's behavior could be numerically simulated using continuation for a finite range of amplitudes A; decreasing A back to its starting value would allow to check if hysteresis occurs, in the case where multiple solutions are obtained.

Leading to an analysis of Newton's cradle, a future step in this research will be considering a string pendulum suspended by two cables attached to a frame which is given an exterior forcing. This is the case of having one ball in the Newton's cradle setup in Fig. 1.1c). The system can be expected to have erratic behavior, given that the strings go alternatively through taut and slack states [16]. The box at the end of Chapter 5 would need to be updated to take into account each string's motion; the equations for both the taut and slack states would have different forms due to the spatial constraint of the second string to which the mass is attached.

If, as in Newton's cradle, multiple balls are considered, then a 3-dimensional version of the equation of motion will be needed. The system would be further complicated by impacts between masses, which would be checked by comparing the x, y, z positions of the masses. If the distance between them is very close to 0, collision occurs and the velocities of the masses would need to be updated using a coefficient of restitution close to 1, such that most of the kinetic energy is conserved (elastic collision).

Appendix A

Preliminary study of the taut-slack 3D pendulum

The analysis in Chapter 5 can be generalized for the 3D pendulum that can be moved by an external forcing in any of the three directions. In the case of a slack string, we will have the similar equations of motion

$$\ddot{x} = 0 \qquad \ddot{y} = 0 \qquad \ddot{z} = -g\,. \tag{A.1}$$

In the taut case we will begin, as before, with the Lagrangian of the system, $\mathcal{L} = T - U - \lambda f$, which equals:

$$\mathcal{L} = \frac{1}{2}m(\dot{x}^2 + \dot{y}^2 + \dot{z}^2) - mgz - \lambda(x^2 + y^2 + z^2 - L^2)\,. \tag{A.2}$$

The Euler equations with respect to $x(t)$, $y(t)$ and $z(t)$ become the equations of motion of the system in the taut case:

$$\ddot{x} = -2\frac{\lambda}{m}x - \beta\dot{x}\,, \tag{A.3a}$$

$$\ddot{y} = -2\frac{\lambda}{m}y - \beta\dot{y}\,, \tag{A.3b}$$

$$\ddot{z} = -g - 2\frac{\lambda}{m}z - \beta\dot{z}\,. \tag{A.3c}$$

We note that our choice of spherical coordinates ensures that we will not have a singularity in the rest state when the pendulum is hanging straight down:

$$x(t) = L\cos\theta\,, \qquad y(t) = L\sin\theta\sin\phi\,, \qquad z(t) = L\sin\theta\cos\phi\,. \tag{A.4}$$

We will use these to eliminate λ and thus determine the equations of motion in terms of known quantities.

By using equations (A.3a) and (A.4) we find that

$$\ddot{x} = -L\left(2\frac{\lambda}{m}\cos\theta - b\dot{\theta}\sin\theta\right)\,.$$

We therefore obtain a first formula for λ:

$$\lambda = \frac{m}{2}(\ddot{\theta}\tan\theta + \dot{\theta}^2 + b\dot{\theta}\tan\theta)\,. \tag{A.5}$$

Now we go on to expressing $\ddot{y}$ from (A.4) and respectively, (A.3b):

$$\ddot{y} = -2\frac{\lambda}{m}L\sin\theta\sin\phi - bL(\dot{\theta}\cos\theta\sin\theta + \dot{\phi}\sin\theta\cos\phi)\,.$$

We get a second formula for λ:

$$\lambda = \frac{m}{2}(-\ddot{\theta}\cot\theta - \ddot{\phi}\cot\phi + \dot{\theta}^2 + \dot{\phi}^2 - 2\dot{\theta}\dot{\phi}\cot\theta\cot\phi - b\dot{\theta}\cot\theta - b\dot{\phi}\cot\phi)\,. \tag{A.6}$$

Finally, from (A.4) and (A.3c) we obtain:

$$\ddot{z} = -g - 2\frac{\lambda}{m} L \sin\theta \cos\phi - bL(\dot{\theta}\cos\theta\cos\phi - \dot{\phi}\sin\theta\sin\phi)\,,$$

which implies

$$\lambda = \frac{m}{2}\left(-\ddot{\theta}\cot\theta + \ddot{\phi}\tan\phi + \dot{\theta}^2 + \dot{\phi}^2 + 2\dot{\theta}\dot{\phi}\cot\theta\tan\phi - b\dot{\theta}\cot\theta + b\dot{\phi}\tan\phi - \frac{g}{L\sin\theta\cos\phi}\right). \tag{A.7}$$

If we set equal the expressions for λ in (A.6) and (A.7), further calculations give us the first angular equation of motion:

$$\ddot{\phi} = -2\dot{\theta}\dot{\phi}\cot\theta - b\dot{\phi} + \left(\frac{g}{L} + \frac{\ddot{\ddot{y}}}{L}\right)\cdot\frac{\sin\phi}{\sin\theta}\,. \tag{A.8}$$

Similarly, by combining equations (A.6) and (A.5), we can find the second equation of motion:

$$\ddot{\theta} = -\frac{g}{L}\cos\theta\cos\phi + \dot{\phi}^2\sin\theta\cos\theta - b\dot{\theta}\,. \tag{A.9}$$

Using either expression of λ and the above equations, we can compute:

$$\lambda = \frac{m}{2}\left(-\frac{g}{L}\sin\theta\cos\phi + \dot{\phi}^2\sin^2\theta + \dot{\theta}^2\right). \tag{A.10}$$

The coordinate changes in (A.4) help us express θ and ϕ as

$$\theta = \arccos\frac{x}{L}$$

and

$$\phi = \arctan\frac{y}{z}\,.$$

Using these changes, λ becomes

$$\lambda = \frac{m}{2}\left(-\frac{gz}{L^2} + \frac{(\dot{y}z - y\dot{z})^2}{L^2(y^2+z^2)} + \frac{\dot{x}^2}{L^2 - z^2}\right), \tag{A.11}$$

and we can finally express the equations of motion in $\ddot{x}$, $\ddot{y}$ and $\ddot{z}$ of the 3D pendulum:

$$\ddot{x} = \frac{gxz}{L^2} - \frac{x(\dot{z}x - z\dot{x})^2}{L^2(y^2+z^2)} - \frac{x\dot{x}^2}{L^2 - x^2} - b\dot{x}\,,$$

$$\ddot{y} = \frac{gyz}{L^2} - \frac{y(\dot{y}z - y\dot{z})^2}{L^2(y^2+z^2)} - \frac{y\dot{x}^2}{L^2 - x^2} - b\dot{y}\,, \tag{A.12}$$

$$\ddot{z} = -g + \frac{gz^2}{L^2} - \frac{z(z\dot{y} - y\dot{z})^2}{L^2(y^2+z^2)} - \frac{z\dot{x}^2}{L^2 - x^2} - b\dot{z}\,.$$

We note that these equations can be checked using a different approach of the Euler-Lagrange method. This approach involves using the Lagrangian as $\mathcal{L} = \frac{m}{2}(\dot{x}^2 + \dot{y}^2 + \dot{z}^2) - mgz$ and Rayleigh's dissipation function for frictional losses:

$$F = \frac{b}{2}(\dot{x}^2 + \dot{y}^2 + \dot{z}^2)\,.$$

Using the same spherical coordinates (A.4) and the extended Euler-Lagrange equations:

$$-\frac{\partial \mathcal{L}}{\partial \theta} + \frac{d}{dt}\left(\frac{\partial \mathcal{L}}{\partial \dot{\theta}}\right) + \frac{\partial F}{\partial \dot{\theta}} = 0\,,$$

and

$$-\frac{\partial \mathcal{L}}{\partial \phi} + \frac{d}{dt}\left(\frac{\partial \mathcal{L}}{\partial \dot{\phi}}\right) + \frac{\partial F}{\partial \dot{\phi}} = 0\,,$$

the same equations of motion are derived.

A similar derivation for equations equivalent to (A.12) for the 2-dimensional case can be performed by considering only the x and z components in equations (A.3) and (A.4). Elimination of λ yields the equations of motion in $\ddot{x}$ and $\ddot{z}$, however implementation of these equations proved to have stability problems. Therefore,

equations (A.12) could have the same issues and would be an interesting aspect to further analyze.

A.1 Switching conditions for the 3D pendulum

As before, equations (A.12) fail to take into account the fact that the string cannot be stretched beyond its maximum length L. Thus, we need to take the same approach as the one used in Chapter 5 for the 2D pendulum.

We begin by choosing one normal vector to the trajectory of the pendulum, as well as two suitable tangential directions $\boldsymbol{t}_1$ and $\boldsymbol{t}_2$:

$$\boldsymbol{n} = (x, y, z),$$

with norm $||\boldsymbol{n}|| = L$.

$$\boldsymbol{t}_1 = (x, y, z - \frac{L^2}{z^2}),$$

for $z \neq 0$ and with norm $||\boldsymbol{t_1}|| = \sqrt{\frac{L^4}{z^2} - L^2}$ and

$$\boldsymbol{t}_2 = \boldsymbol{n} \times \boldsymbol{t}_1 = (-\frac{y}{z}L^2, \frac{x}{z}L^2, 0),$$

with norm $||\boldsymbol{t_2}|| = L^2\sqrt{\frac{x^2+y^2}{z^2}}$.

We begin with the velocity vector just before the taut position:

$$\boldsymbol{v}^- = (\dot{x}, \dot{y}, \dot{z}) = v_n^-\boldsymbol{n} + v_{t_1}^-\boldsymbol{t}_1 + v_{t_2}^-\boldsymbol{t}_2\,,$$

and thus we can derive $\boldsymbol{v}_n^-$, $\boldsymbol{v}_{t_1}^-$ and $\boldsymbol{v}_{t_2}^-$ by finding the projections of $\boldsymbol{v}-$ on the normal and tangential directions:

$$\boldsymbol{v}_n^- = \frac{\boldsymbol{v}^- \cdot \boldsymbol{n}}{||\boldsymbol{n}||^2}\boldsymbol{n} = \frac{x\dot{x} + y\dot{y} + z\dot{z}}{L^2}\boldsymbol{n}\,, \tag{A.13a}$$

$$\boldsymbol{v}_{t_1}^- = \frac{\boldsymbol{v}^- \cdot \boldsymbol{t}_1}{||\boldsymbol{t_1}||^2}\boldsymbol{t}_1 = \frac{x\dot{x} + y\dot{y} + \left(z - \frac{L^2}{z}\right)\dot{z}}{L^2}\left(\frac{L^2}{z^2} - 1\right)\boldsymbol{t}_1\,, \tag{A.13b}$$

$$\boldsymbol{v}_{t_2}^- = \frac{\boldsymbol{v}^- \cdot \boldsymbol{t}_2}{||\boldsymbol{t_2}||^2}\boldsymbol{t}_2 = \frac{-yz\dot{x} + xz\dot{y}}{L^2(x^2+y^2)}\boldsymbol{t}_2\,. \tag{A.13c}$$

Since $\boldsymbol{v}^+ = (\dot{x}^+, \dot{y}^+, \dot{z}^+) = v_n^+\boldsymbol{n} + v_{t_1}^+\boldsymbol{t}_1 + v_{t_2}^+\boldsymbol{t}_2$. we would obtain equations identically similar to equations (A.13) for the components of the velocity right after the taut position. Our physical understanding of the system dictates that the following changes need to be incorporated in the simulation if the velocity at the taut position is positive:

$$v_n^+ = 0 \qquad v_{t_1}^+ = v_{t_1}^- \qquad v_{t_2}^+ = v_{t_2}^-\,. \tag{A.14}$$

This implies the following system of equations:

$$x\dot{x}^+ + y\dot{y}^+ + z\dot{z}^+ = 0\,, \tag{A.15a}$$

$$x\dot{x}^+ + y\dot{y}^+ + \left(z - \frac{L^2}{z^2}\right)\dot{z}^+ = x\dot{z} + y\dot{y} + \left(z - \frac{L^2}{z^2}\right)\dot{z}\,, \tag{A.15b}$$

$$-y\dot{x}^+ + x\dot{y}^+ = -y\dot{x} + x\dot{y}\,. \tag{A.15c}$$

This system of equations can be solved for unknowns $\dot{x}^+$, $\dot{y}^+$ and $\dot{z}^+$:

$$\dot{x}^+ = \frac{1}{x^2+y^2}\left[\dot{x}\left(\frac{x^2z^2}{L^2} + y^2\right) + \dot{y}\left(\frac{xyz^2}{L^2} - xy\right) + \dot{z}xz(z^2 - L^2)\right]\,,$$

$$\dot{y}^+ = \frac{1}{x^2+y^2}\left[\dot{x}\left(\frac{xyz^2}{L^2} - xy\right) + \dot{y}\left(\frac{y^2z^2}{L^2} + x^2\right) + \dot{z}yz(z^2 - L^2)\right]\,, \tag{A.16}$$

$$\dot{z}^{+} = \frac{1}{L^2}[-\dot{x}xz - \dot{y}yz - \dot{z}(z^2 - L^2)]\,.$$

Bibliography

[1] M. V. Bartuccelli, G. Gentile, and K. V. Georgiou, *On the dynamics of a vertically driven damped planar pendulum*, Proceedings: Mathematical, Physical and Engineering Sciences, 457 (2001), pp. 3007–3022.

[2] F. Christiansen and H. H. Rugh, *Computing Lyapunov spectra with continuous Gram-Schmidt orthonormalization*, Nonlinearity, 16 (1997), pp. 1063–1072.

[3] T. Gilet, N. Vandewalle, and S. Dorbolo, *Completely inelastic ball*, Physical Review E, 79 (2009), pp. 055201 1–4.

[4] H. Goldstein, *Classical Mechanics*, Addison-Wesley Pub. Co., 1980.

[5] A. Goriely, P. Boulanger, and J. Leroy, *Toy models: The jumping pendulum*, American Journal of Physics, 74 (2006), pp. 784–788.

[6] L. D. Humphreys and P. J. McKenna, *When a Mechanical Model goes Nonlinear: Unexpected Responses to Low-Periodic Shaking*, the American Mathematical Monthly, 112 (2005), pp. 861–875.

[7] D. W. Jordan and P. Smith, *Nonlinear Ordinary Differential Equations: An Introduction to Dynamical Systems*, Oxford University Press, 1999.

[8] J. B. Keller, *Ponytail motion*, Society for Industrial and Applied Mathematics, 70 (2010), pp. 2667–2672.

[9] J. B. Marion and S. T. Thornton, *Classical dynamics of particles and systems*, Saunders College Publishing, Harcourt Brace College Publishers, 4th ed., 1995.

[10] D. Morin, *Introduction to Classical Mechanics*, Cambridge University Press, 2007.

[11] E. R. Pinch, *Optimal Control and the Calculus of Variations*, Oxford University Press, 1993.

[12] K. Popp, *Non-smooth mechanical systems*, Journal of Applied Mathematics and Mechanics, 64 (2000), pp. 765–772.

[13] W. H. Press, *Numerical recipes in C: the art of scientific computing*, Cambridge University Press, 1997.

[14] C. Sangwin, *Modelling the journey from elementary word problems to mathematical research*, Notices of the AMS, 58 (2011), pp. 1436–1445.

[15] S. H. Strogatz, *Nonlinear dynamics and chaos : with applications to physics, biology, chemistry, and engineering*, Perseus Pub., 1994.

[16] L. N. Virgin, J. Nichols, W. Simmons, and R. Plaut, *On the response of a shaken cable-suspended mass*, ASME Design Engineering Technical Conference, (2001).

[17] A. Wolf, J. B. Swift, H. L. Swinney, and J. A. Vastano, *Determining Lyapunov exponents from a time series*, Physica D, 0545 (1985), pp. 285–317.